Ultrasensitive N-Photon Interferometric Autocorrelator

Zili Zhou (周子理),[1,*] Giulia Frucci,[1] Francesco Mattioli,[2] Alessandro Gaggero,[2]
Roberto Leoni,[2] Saeedeh Jahanmirinejad,[1] Thang Ba Hoang,[1] and Andrea Fiore[1]
[1]*COBRA Research Institute, Eindhoven University of Technology, P.O. Box 513, 5600 MB Eindhoven, The Netherlands*
[2]*Istituto di Fotonica e Nanotecnologie (IFN), CNR, via Cineto Romano 42, 00156 Rome, Italy*
(Received 23 August 2012; published 28 March 2013)

We demonstrate a novel method to measure Nth-order ($N = 1, 2, 3, 4$) interferometric autocorrelation with high sensitivity and temporal resolution. It is based on the combination of linear absorption and nonlinear detection in a superconducting nanodetector, providing much higher efficiency than methods based on all-optical nonlinearities. Its temporal resolution is only limited by the quasiparticle energy relaxation time, which is directly measured to be in the 20 ps range for the NbN films used in this work. We present a general model of interferometric autocorrelation with these nonlinear detectors and discuss the comparison with other approaches and possible improvements.

DOI: 10.1103/PhysRevLett.110.133605 PACS numbers: 42.50.−p, 42.65.−k, 85.25.Oj

The temporal correlation functions of various orders are of fundamental importance in the classical and quantum description of optical fields. The first-order (field) autocorrelation function describes temporal coherence and therefore spectral linewidth, and second-order (intensity) autocorrelation is used to measure the temporal properties of pulsed sources and to distinguish quantum and classical fields, whereas the measurement of higher-order autocorrelation is more sensitive to coherence features (e.g., photon bunching) of the light field [1] and can be used to determine the asymmetry of light pulses [2]. Whereas the first-order autocorrelation function is easily measured using an interferometer and a linear detector [3], the measurement of higher-order correlation functions requires a process that is nonlinear in the intensity $I(t)$. In interferometric autocorrelators, the normalized second-order correlation function $g^{(2)}(\tau) = \langle I(t)I(t+\tau)\rangle/\langle I(t)\rangle^2$ is usually measured by using either second-harmonic generation (SHG) in a nonlinear crystal, followed by a linear detector [4], or two-photon absorption (TPA) in the detector itself [5,6]. In both cases, the detector measures the square of the total intensity at the output of the interferometer $\langle I_{\mathrm{tot}}^2(t)\rangle \propto \langle I^2(t)\rangle + 2\langle I(t)I(t+\tau_d)\rangle$ where τ_d is the delay between the two arms of the interferometer, together with interference terms which are sensitive to the phase properties of the beam. While these approaches offer very high temporal resolution, since the related processes are nearly instantaneous, their sensitivity is limited by the low nonlinear susceptibilities involved in the SHG or TPA processes. Because of the even lower relevance of higher-order optical nonlinearities, measurement of the autocorrelations of order $N > 2$ requires very high input powers [2,7,8]. An alternative approach consists of combining linear optical detection with nonlinear processing in the electrical readout, e.g., in a correlation card, as in the Hanbury Brown-Twiss interferometer [9]. In this case, sensitive single-photon detectors can be used; however, the temporal resolution is limited to ≥ 50 ps by the jitter of the detector output and the amplification and correlation electronics [10]. In addition, different from interferometric autocorrelation, these approaches do not provide any information on the phase properties.

In this Letter, we report a novel approach to the measurement of the interferometric autocorrelation of order $N \geq 2$, which is based on the combination of linear absorption and nonlinear detection in a single device. The general principle consists of absorbing incident photons in a linear absorber (i.e., a material where the absorption probability per unit time is proportional to light intensity), which produces an output pulse only if two or more photons are absorbed within a certain time interval in the femtosecond or picosecond range. We show the implementation of this concept in a superconducting nanodetector (ND) where the nonlinearity is widely tunable by varying the bias current. We directly measure the temporal dynamics of the nonlinearity in the picosecond range, and we attribute it to the relaxation dynamics of photo-created quasiparticles (QPs). We show its application to the measurement of up to fourth-order interferometric autocorrelation, observing an extremely high sensitivity related to the linear absorption process and to the low detector noise.

The superconducting nanodetector consists of a nanoscale constriction in a superconducting wire (see Fig. 1). The device used in this work is based on a 4.3 nm-thick NbN film (critical temperature $T_c = 10.2$ K) sputtered on GaAs substrate and has a constriction size of about 150 nm, patterned by electron beam lithography and reactive-ion etching. The nanodetector is biased with a current I_b smaller than the superconducting critical current I_c. Similarly to nanowire superconducting single-photon detectors [12], the absorption of one or more photons produces a nonequilibrium population of QPs in the nanodetector's active region, locally suppressing the superconductivity and increasing the probability of vortex crossing, which can result in the transition to the normal state [13,14]. The detection probability is a strong function of

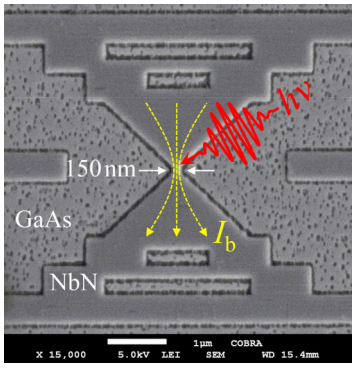

FIG. 1 (color online). Scanning electron microscope image of a NbN superconducting nanodetector.

the absorbed energy (i.e., to the number of photons) and of the bias current I_b so that the nanodetector can be set to respond to $\geq N$ photons by choosing I_b [15,16].

In this study, we focus on the temporal characteristics of the nanodetector's multiphoton response and on its application as an interferometric autocorrelator. As we focus here on the application to the characterization of classical light sources, we describe the detection process as a sequence of single-photon absorption events using the semiclassical photodetection theory. Assuming an incident light pulse with cycle-average intensity $I_{\rm in}(t)$ on the nanodetector, the probability of creating a hot spot within a time interval $(t, t + dt)$ is equal to $\zeta S I_{\rm in}(t)dt$, where ζ is related to the absorbance $\eta_{\rm abs}$ by $\zeta = \eta_{\rm abs}/h\nu$ and S is the active area. In the two-photon regime, for example, the click probability $P_{\rm click}$ (assumed $\ll 1$) is equal to the probability that two photons are absorbed, weighted by a function $\eta(\tau_{12})$ of the time difference τ_{12} between absorption of the first and the second photon at times t_1 and t_2, respectively,

$$P_{\rm click} = \int_{-\infty}^{+\infty}\int_{-\infty}^{+\infty} \eta(t_2 - t_1)\zeta S I_{\rm in}(t_1)\zeta S I_{\rm in}(t_2)dt_1 dt_2 = \zeta^2 S^2 \int_{-\infty}^{+\infty} \eta(\tau_{12}) \int_{-\infty}^{+\infty} I_{\rm in}(t) I_{\rm in}(t + \tau_{12})dt d\tau_{12}. \quad (1)$$

The $\eta(\tau_{12})$ function, named the nonlinear response function (NRF) in the following, depends on the QP dynamics in the superconductor and determines the intrinsic response time $\tau_{\rm ND}$ of the nanodetector. The value of $\eta(\tau_{12})$ is expected to decay from a maximum value of $\eta(0)$ (which depends on I_b) to 0 for $\tau_{12} \gg \tau_{\rm ND}$. In general, the detection probability in the N-photon regime ($N \geq 2$) is

$$P_{\rm click} = \zeta^N S^N \int_{-\infty}^{+\infty} \eta_N(\tau_{1N}, \tau_{2N}, \ldots, \tau_{N-1,N}) \times \int_{-\infty}^{+\infty} I_{\rm in}(t) I_{\rm in}(t + \tau_{1N}) I_{\rm in}(t + \tau_{2N}) \ldots \times I_{\rm in}(t + \tau_{N-1,N}) dt d\tau_{1N} d\tau_{2N} \ldots d\tau_{N-1,N}, \quad (2)$$

where $\tau_{iN} = t_N - t_i$ denotes the difference between the absorption times of the ith and the last photon.

When the incident pulse width is much larger than $\tau_{\rm ND}$, Eq. (2) is approximated as $P_{\rm click} \propto \int_{-\infty}^{+\infty} I_{\rm in}^N(t)dt$. When a nanodetector is placed at the output of a Michelson interferometer, the input intensity reads $I_{\rm in}(t) \propto |E(t) + E(t + \tau_d)|^2$ and the $P_{\rm click}$ in the N-photon regime is proportional to the Nth-order interferometric autocorrelations given by $P_{\rm click}(\tau_d) \propto \int_{-\infty}^{+\infty}[|E(t) + E(t + \tau_d)|^2]^N dt$. In the two-photon regime, by filtering out the interference terms we obtain $P_{\rm click}(\tau_d) \propto \langle I^2(t)\rangle + 2\langle I(t)I(t + \tau_d)\rangle$ and, therefore, the $g^{(2)}(\tau_d)$, similarly to the SHG- and TPA-based autocorrelators.

The NRF can be measured by probing the autocorrelator with short pulses. For a pulse duration much shorter than $\tau_{\rm ND}$, the response of the nanodetector placed at the output of a Michelson interferometer can be found from Eq. (2). In the two-photon regime, for example, after filtering out the interference terms, Eq. (1) becomes $P_{\rm click}(\tau_d) \propto \eta(0) + \eta(\tau_d) + f(\tau_d)$ (see Supplemental Material [17]). The function $f(\tau_d)$ depends on the degree of first-order coherence of the input light and is different from zero only for delays shorter than the coherence time. For longer delays, the $P_{\rm click}(\tau_d)$, normalized by its value at $\tau_d \gg \tau_{\rm ND}$, is expected to vary as $P_{\rm click}(\tau_d)/P_{\rm click}(\infty) = 1 + \eta(\tau_d)/\eta(0)$ so that the NRF and therefore the autocorrelator's timing resolution can be measured.

The NRF was first measured by sending 1.6 ps pulses from an optical parametric oscillator (OPO) at $\lambda = 1.13\,\mu$m into a fiber-based Michelson interferometer and then to a nanodetector held at a temperature of 1.2 K using a lensed fiber producing a spot with an e^{-2} diameter of 5 μm. The delay τ_d in the interferometer is controlled by a motorized delay line (coarse control) and a fiber stretcher (fine control). The I_c of the device was about 26 μA. During the measurement, the nanodetector was set in different photon regimes by choosing a proper I_b. As shown in Fig. 2(a), the count rate (CR) was measured as a function of the light power at different I_b values. The solid lines with slopes of 1.04, 2.06, 3.06, and 3.99 are the fits to the measured data

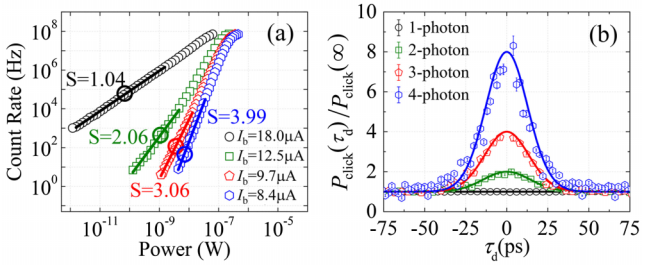

FIG. 2 (color online). (a) CR as a function of the light power for different I_b values. The fitting lines with slopes of 1.04, 2.06, 3.06, and 3.99 indicate the one-, two-, three-, and four-photon regimes, respectively. (b) Normalized CR as a function of τ_d, measured when the detector was working at the four chosen points [marked by large circles in (a)]. The solid lines are calculation results (see text).

in log-log scale in the power ranges where the one-, two-, three-, and four-photon response was dominant [15]. We chose one point at each of the four photon regimes and measured the CR as a function of τ_d, normalized by its values at long delays, as shown in Fig. 2(b). The data points near $\tau_d = 0$, where the measured autocorrelation is sensitive to the first-order coherence, are not shown in the plot and were not considered in the fit since they introduce additional fitting error (see Supplemental Material [17]). At $I_b = 18.0$ μA, the CR is independent of the delay since the detector is working in the linear regime. When the I_b was lowered to 12.5, 9.7, and 8.4 μA (corresponding to the two-, three-, and four-photon regimes, respectively), a maximum was observed at zero delay. Since the width of these peaks is much wider than the OPO pulse width, the measurement probes the intrinsic response of the detector. In particular, the two-photon normalized response in Fig. 2(b) directly provides the $1 + \eta(\tau_d)/\eta(0)$ dependence. The $\eta(\tau)$ value is determined by the thermalization and relaxation processes of the photocreated QP and by the functional dependence of P_{click} on the QP concentration [13,14]. Indeed, the QP population first grows as the electron population thermalizes via electron-electron scattering, in a time scale of a few ps, then decays due to electron-photon interaction and phonons escaping to the substrate [18]. This QP decay is expected to determine the τ_{ND} value in the N-photon regime, since the I_b is chosen so that P_{click} is high only when all QP produced by the N photons are present at the same time. As P_{click} is a strong function of the QP number, involving many microscopic parameters, a fit of the measured $\eta(\tau)$ using a microscopic model would not be reliable. Instead, we introduce an empirical Gaussian NRF defined as $\eta(\tau_{12}) = \eta(0)\exp[-(\tau_{12}/\tau_{\text{ND}})^2]$. The fits to 10 measured two-photon autocorrelation traces provide a τ_{ND} value of 20.4 ± 0.8 ps [19]. To fit the $N > 2$ traces, we further assume that the multiphoton response factorizes as $\eta_N(\tau_{1N}, \tau_{2N}, \ldots, \tau_{N-1,N}) = \eta(\tau_{1N})\eta(\tau_{2N}) \ldots \eta(\tau_{N-1,N})$. This is reasonable if one assumes that η_N has an approximately exponential dependence on the total QP concentration after absorption of the Nth photon, as suggested by the vortex-assisted photodetection model [13,14], and that the QP relaxation time does not depend on QP concentration. Using the τ_{ND} value extracted from the two-photon autocorrelation traces as described above, $P_{\text{click}}(\tau_d)$ was calculated for the three- and four-photon regimes from Eq. (2) without additional fitting parameters and shows excellent agreement with the experiment [Fig. 2(b)], which provides strong experimental support to our model.

With knowledge of the temporal resolution, autocorrelation experiments were performed on pulses generated by a gain-switched 1.3 μm diode laser with 10 MHz repetition rate and about 70 ps pulse width. The one-, two-, three-, and four-photon regimes were first found by choosing different I_b values. At each I_b, CRs were recorded as a function of τ_d in the N-photon ($N = 1, 2, 3, 4$) regime as shown in Figs. 3(a)–3(d), respectively. The fringe contrast ratio is observed to increase with N, in good agreement with the theoretical values of 2, 8, 32, and 128 for $N = 1, 2, 3$, and 4, respectively. In the one-photon regime [Fig. 3(a)], the normalized first-order autocorrelation function $g^{(1)}(\tau_d)$ was calculated from the visibility of the interference fringes [3]. For $N > 1$, higher-order intensity autocorrelation traces were obtained by applying a low-pass filter to the interferograms in Figs. 3(b)–3(d). In order to explain the experimental results, we assumed that the incident light was a Gaussian pulse with a linear chirp. The electric field is modeled as $E(t) = E_0 \exp[-4\ln(2)(1 + iA)t^2/\tau_p^2]$, where E_0 is the field amplitude, A is the linear chirp parameter [22], and τ_p is the full width at half maximum (FWHM) of the pulse. By fitting the measured $|g^{(1)}(\tau_d)|$ in Fig. 3(a) together with the second-order intensity autocorrelation (low-pass trace) in Fig. 3(b), A and τ_p were determined to be 5.3 and 70.6 ps. The third- and fourth-order interferometric autocorrelations were then calculated based on

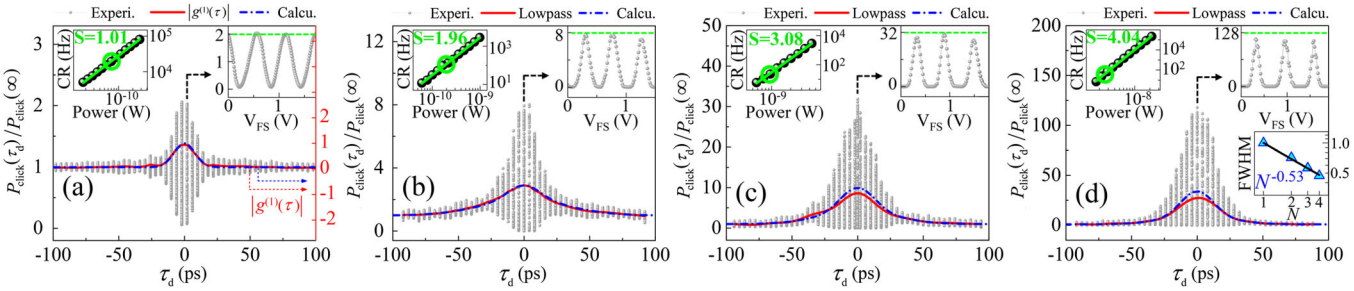

FIG. 3 (color online). (a)–(d) Normalized CR as a function of τ_d in the different regimes at I_b of 18.0, 14.0, 11.5, and 9.6 μA respectively. The $|g^{(1)}(\tau_d)|$ [solid red line in (a)] and low-pass curves [solid red lines in (b)–(d)] agree well with the calculations (dash-dotted blue lines). Upper-left insets: CR as a function of incident power in log-log scale. The fitting slopes of 1.01, 1.96, 3.08, and 4.04 indicate the one-, two-, three-, and four-photon regimes, respectively. The green circles indicate the points chosen for the measurements in the main panel. Upper-right insets: Expanded view of the interference fringes at small delays, plotted as a function of the voltage V_{FS} applied to the fiber stretcher. Lower-right inset in (d): FWHM of the fringes normalized by their period extracted from the upper-right insets in (a)–(d) as a function of N, showing a $1/\sqrt{N}$ dependence.

Eq. (2) without additional fitting parameters. Their low-pass traces show a good agreement with the experiments, considering the very simplified assumption for the chirp. An enlarged view of each interferogram is shown as an upper-right inset in each panel of Fig. 3, showing a clear narrowing of the fringes for increasing N. As shown in the lower-right inset of Fig. 3(d), the FWHM of the fringes normalized by their period scales as approximately $1/\sqrt{N}$, which is a characteristic of multiphoton interferometry [23] and further confirms our conclusions.

The nanodetector-based autocorrelator provides much higher sensitivity as compared to conventional autocorrelators. The two-photon autocorrelation trace in Fig. 3(b) was taken at $P_{\mathrm{pk}}P_{\mathrm{av}} = 5.6 \times 10^{-17}$ W^2 (P_{pk} is the peak power, and P_{av} is the average power), about 7 orders of magnitude lower than the minimum reported $P_{\mathrm{pk}}P_{\mathrm{av}}$ based on TPA [24] and about 2 orders of magnitude lower than the lowest $P_{\mathrm{pk}}P_{\mathrm{av}}$ using SHG [25]. For input pulses longer than τ_{ND}, Eq. (2) can be written as $P_{\mathrm{click}} = C_{\mathrm{ND}} \int_{-\infty}^{+\infty} P_{\mathrm{in}}^2(t)dt$, where $P_{\mathrm{in}} = I_{\mathrm{in}}S$ is the incident power and $C_{\mathrm{ND}} = \sqrt{\pi}\eta_{\mathrm{abs}}^2\eta(0)\tau_{\mathrm{ND}}/(h\nu)^2$ represents a nonlinear response efficiency. Using the measured values of $\eta_{\mathrm{abs}} = 1.5 \times 10^{-4}$, $\eta(0) \approx 0.5$ [16], and dark count rate $R_{\mathrm{dark}} = 1$ Hz, we derive a sensitivity of $P_{\mathrm{pk}}^{\mathrm{min}}P_{\mathrm{av}}^{\mathrm{min}} \approx 5.8 \times 10^{-20}$ W^2 (see Supplemental Material [17]), corresponding to ~4 photons/pulse in our experiment. In a higher-photon regime, the advantage of using linear absorption is even larger. Indeed, the three-photon autocorrelation shown in Fig. 3(c) was performed at an average power of about 1 nW, corresponding to $P_{\mathrm{pk}}^2P_{\mathrm{av}} \approx 2.0 \times 10^{-21}$ W^3, an improvement of about 21 orders of magnitude over that in Ref. [26]. To the best of our knowledge, N-photon interferometric autocorrelation for $N > 3$ has not been reported before. As compared to autocorrelators based on spatial coupling of the optical beam to multiple single-photon detectors and electronic correlation [27], our nanodetector provides higher temporal resolution, much easier readout, and phase information.

The very high nonlinear response of the nanodetector can be directly traced to the finite size and time duration of the hot spot created by the real absorption of one photon, as compared to the virtual transitions involved in TPA. Indeed, a two-photon detection is triggered if the second photon is absorbed within the volume and time duration of the hot spot created by the first photon. This shows that a compromise exists between C_{ND} and τ_{ND}: for the nanodetector, the τ_{ND} value is determined by the QP relaxation time while in TPA it is related to the lifetime of the virtual states associated to the TPA transition, on the order of femtoseconds [6]. A similar compromise exists in SHG-based autocorrelators, where higher conversion efficiency requires a longer SHG crystal translating into a smaller phase-matching bandwidth and lower temporal resolution τ_{res} [28,29]. Defining $P_{\mathrm{pk}}P_{\mathrm{av}}\tau_{\mathrm{res}}$ as a figure of merit, the present nanodetector is about 2 orders of magnitude better than the record using TPA [24] and comparable with the record based on SHG, where much higher experimental complexity is required [25]. We note that a key advantage as compared to SHG-based autocorrelators is the nanodetector's large wavelength range, limited only by the requirement to operate in the desired N-photon regime, which can be easily adjusted by varying the I_b. This, in principle, enables the measurement of interferometric autocorrelation from the visible to the mid-infrared wavelengths.

The sensitivity of our autocorrelator is presently limited by the low η_{abs} value related to the spatial mismatch between the incoming beam and the nanodetector's active area and to the small thickness of the NbN film. By focusing the beam with a high-numerical aperture lens, we can achieve a much higher absorbance $\eta_{\mathrm{abs}} \approx 10^{-2}$ [30]. The integration of a plasmonic antenna and a bottom reflector [31] could increase η_{abs} to the 10^{-1} range, leading to $P_{\mathrm{pk}}^{\mathrm{min}}P_{\mathrm{av}}^{\mathrm{min}} \approx 10^{-25}$ W^2 for the two-photon autocorrelation. On the other hand, increasing the detector area (as done in meander nanowire detectors [32]) results in $\eta_{\mathrm{abs}} \propto L$ and $\eta(0) \propto l_{\mathrm{hs}}/L$ (L is the nanowire length, and l_{hs} is the hot spot length) so that C_{ND} scales linearly with η_{abs}. The nanoscale nature of the detector is therefore crucial to reaching the ultimate sensitivity. Finally, we note that the 20 ps temporal resolution in our experiments is limited to the QP relaxation time in NbN films and could be much improved using different superconducting materials, such as high-T_c Y-Ba-Cu-O films, where relaxation times ~1 ps were observed [33], opening the way to the characterization of Nth-order correlation functions in a few-ps range with unprecedented sensitivity.

The authors gratefully thank Professor E. Rosencher and J. J. Renema, Dr. M. J. A. de Dood and Dr. M. P. van Exter for enlightening discussions, D. Sahin for taking the SEM picture (Fig. 1), Dr. J. E. M. Haverkort and S. Mokhlespour for assistance in operating the OPO system, and T. Xia and F. M. Pagliano for technical help. This work is part of the research program of the Foundation for Fundamental Research on Matter, which is financially supported by the Netherlands Organisation for Scientific Research, and is also supported by NanoNextNL, a micro- and nanotechnology program of the Dutch Ministry of Economic Affairs and Agriculture and Innovation and 130 partners, and by the European Commission through FP7 project Q-ESSENCE (Contract No. 248095).

Note added.—After submission of this Letter, a QP relaxation time of about 15 ps, measured using a different experimental technique in NbN meander nanowire detectors on a different substrate, was reported in Ref. [34].

*Corresponding author.
z.zhou@tue.nl

[1] M. Aßmann, F. Veit, M. Bayer, M. van der Poel, and J. M. Hvam, Science **325**, 297 (2009).

[2] P. Langlois and E. P. Ippen, Opt. Lett. **24**, 1868 (1999).

[3] M. Fox, *Quantum Optics: An Introduction* (Oxford University Press, New York, 2006), Chapter 2.

[4] H. P. Weber, J. Appl. Phys. **38**, 2231 (1967).

[5] B. R. Mollow, Phys. Rev. **175**, 1555 (1968).

[6] F. Boitier, A. Godard, E. Rosencher, and C. Fabre, Nat. Phys. **5**, 267 (2009).

[7] D. Meshulach, Y. Barad, and Y. Silberberg, J. Opt. Soc. Am. B **14**, 2122 (1997).

[8] D. H. Auston, Appl. Phys. Lett. **18**, 249 (1971).

[9] R. Hanbury Brown and R. Q. Twiss, Nature (London) **177**, 27 (1956); R. Hanbury Brown and R. Q. Twiss, Nature (London) **178**, 1046 (1956).

[10] The fast correlation technique demonstrated in Refs. [1,11] also belongs to this category but suffers from the low sensitivity of streak cameras in the near-infrared region.

[11] J. Wiersig *et al.*, Nature (London) **460**, 245 (2009).

[12] G. N. Gol'tsman, O. Okunev, G. Chulkova, A. Lipatov, A. Semenov, K. Smirnov, B. Voronov, A. Dzardanov, C. Williams, and R. Sobolewski, Appl. Phys. Lett. **79**, 705 (2001).

[13] A. D. Semenov, P. Haas, H.-W. Hübers, K. Ilin, M. Siegel, A. Kirste, T. Schurig, and A. Engel, Physica (Amsterdam) **C468**, 627 (2008).

[14] L. N. Bulaevskii, M. J. Graf, and V. G. Kogan, Phys. Rev. B **85**, 014505 (2012).

[15] D. Bitauld, F. Marsili, A. Gaggero, F. Mattioli, R. Leoni, S. J. Nejad, F. Levy, and A. Fiore, Nano Lett. **10**, 2977 (2010).

[16] J. J. Renema, G. Frucci, Z. Zhou, F. Mattioli, A. Gaggero, R. Leoni, M. J. A. de Dood, A. Fiore, and M. P. van Exter, Opt. Express **20**, 2806 (2012).

[17] See the Supplemental Material at http://link.aps.org/supplemental/10.1103/PhysRevLett.110.133605 for a detailed discussion on probing the nanodetector's intrinsic response in the two-photon regime, and for more details on the sensitivity comparison to conventional autocorrelators.

[18] A. D. Semenov, G. N. Gol'tsman, and A. A. Korneev, Physica (Amsterdam) **C351**, 349 (2001).

[19] This value is comparable but shorter than the hot-electron energy relaxation time in a NbN microbridge measured by electro-optic sampling [20] and by terahertz spectroscopy [21]; this difference may be related to the difference in film thickness and film properties.

[20] K. S. Il'in, M. Lindgren, M. Currie, A. D. Semenov, G. N. Gol'tsman, R. Sobolewski, S. I. Cherednichenko, and E. M. Gershenzon, Appl. Phys. Lett. **76**, 2752 (2000).

[21] M. Beck, M. Klammer, S. Lang, P. Leiderer, V. V. Kabanov, G. N. Gol'tsman, and J. Demsar, Phys. Rev. Lett. **107**, 177007 (2011).

[22] J. C. M. Diels, J. J. Fontaine, I. C. McMichael, and F. Simoni, Appl. Opt. **24**, 1270 (1985).

[23] E. Yablonovitch and R. B. Vrijen, Opt. Eng. (N.Y.) **38**, 334 (1999).

[24] L. P. Barry, B. C. Thomsen, J. M. Dudley, and J. D. Harvey, Electron. Lett. **34**, 358 (1998).

[25] C. S. Hsu, H.-C. Chiang, H.-P. Chuang, C.-B. Huang, and S.-D. Yang, Opt. Lett. **36**, 2611 (2011).

[26] Y. Wei, S. Howard, A. Straub, Z. Wang, J. Cheng, S. Gao, and C. Xu, Opt. Lett. **36**, 2372 (2011).

[27] M. J. Stevens, B. Baek, E. A. Dauler, A. J. Kerman, R. J. Molnar, S. A. Hamilton, K. K. Berggren, Richard P. Mirin, and S. W. Nam, Opt. Express **18**, 1430 (2010).

[28] A. M. Weiner, IEEE J. Quantum Electron. **19**, 1276 (1983).

[29] S. D. Yang, H. Miao, Z. Jiang, A. M. Weiner, K. R. Parameswaran, and M. M. Fejer, Appl. Opt. **46**, 6759 (2007).

[30] This value is obtained by assuming that the diameter of the Gaussian beam spot decreases from 5 to 0.5 μm by using a high-numerical aperture lens and the nanodetector's active area is 150 nm $\times$ 150 nm.

[31] A. Gaggero *et al.*, Appl. Phys. Lett. **97**, 151108 (2010).

[32] A. Verevkin, J. Zhang, R. Sobolewski, A. Lipatov, O. Okunev, G. Chulkova, A. Korneev, K. Smirnov, G. N. Gol'tsman, and A. Semenov, Appl. Phys. Lett. **80**, 4687 (2002).

[33] M. Lindgren, M. Currie, C. A. Williams, T. Y. Hsiang, P. M. Fauchet, R. Sobolewski, S. H. Moffat, R. A. Hughes, J. S. Preston, and F. A. Hegmann, IEEE J. Sel. Top. Quantum Electron. **2**, 668 (1996).

[34] R. W. Heeres and V. Zwiller, Appl. Phys. Lett. **101**, 112603 (2012).